BRAIN
ORIGINAL ARTICLE

Reduced endothelial caveolin-1 underlies deficits in brain insulin signalling in type 2 diabetes

Aashutosh U. Shetti,[1] Abhirami Ramakrishnan,[1] Liudmila Romanova,[2] Wenping Li,[3] Khanh Vo,[1] Ipsita Volety,[1] Ishara Ratnayake,[4] Terilyn Stephen,[1] Richard D. Minshall,[5,6] Stephanie M. Cologna[3] and Orly Lazarov[1]

Patients with type 2 diabetes exhibit severe impairments in insulin signalling in the brain and are five times more likely to develop Alzheimer's disease. However, what leads to these impairments is not fully understood.
Here, we show reduced expression of endothelial cell caveolin-1 (Cav-1) in the *db/db* (*Lepr*^{db}) mouse model of type 2 diabetes. This reduction correlated with alterations in insulin receptor expression and signalling in brain microvessels as well as brain parenchyma. These findings were recapitulated in the brains of endothelial cell-specific Cav-1 knock-out (Tie2Cre; Cav-1$^{fl/fl}$) mice. Lack of Cav-1 in endothelial cells led to reduced response to insulin as well as reduced insulin uptake. Furthermore, we observed that Cav-1 was necessary for the stabilization of insulin receptors in lipid rafts. Interactome analysis revealed that insulin receptor interacts with Cav-1 and caveolae-associated proteins, insulin-degrading enzyme and the tight junction protein Zonula Occludence-1 in brain endothelial cells. Restoration of Cav-1 in Cav-1 knock-out brain endothelial cells rescued insulin receptor expression and localization.
Overall, these results suggest that Cav-1 regulates insulin signalling and uptake by brain endothelial cells by modulating IR-α and IR-β localization and function in lipid rafts. Furthermore, depletion of endothelial cell–specific Cav-1 and the resulting impairment in insulin transport leads to alteration in insulin signalling in the brain parenchyma of type 2 diabetics.

1 Department of Anatomy and Cell Biology, College of Medicine, The University of Illinois Chicago, Chicago, IL 60612, USA
2 Department of Neurological Sciences, Rush University Medical Center, Chicago, IL 60612, USA
3 Department of Chemistry, College of Liberal Arts and Sciences, The University of Illinois Chicago, Chicago, IL 60612, USA
4 Electron Microscopy Core, Research Resource Center, The University of Illinois Chicago, Chicago, IL 60612, USA
5 Department of Pharmacology and Regenerative Medicine, College of Medicine, The University of Illinois Chicago, Chicago, IL 60612, USA
6 Department of Anesthesiology, College of Medicine, The University of Illinois Chicago, Chicago, IL 60612, USA

Correspondence to: Dr Orly Lazarov, PhD
Department of Anatomy and Cell Biology, The University of Illinois Chicago,
578 CME (M/C 512), 808 South Wood Street
Chicago, IL 60612, USA
E-mail: olazarov@uic.edu

Correspondence may also be addressed to: Dr Richard D. Minshall, PhD
Department of Anatomy and Cell Biology, The University of Illinois Chicago,
E403 MSB (M/C 868), 835 South Wolcott Avenue
Chicago, IL 60612, USA
E-mail: rminsh@uic.edu

Received August 05, 2022. Revised January 07, 2023. Accepted January 17, 2023. Advance access publication February 3, 2023
Published by Oxford University Press on behalf of the Guarantors of Brain 2023.

Keywords: caveolin-1; insulin; type 2 diabetes; cerebrovasculature; endothelial cells; Alzheimer's disease

Introduction

Type 2 diabetes mellitus (T2DM) is a metabolic disorder characterized by insulin resistance and pancreatic β-cell dysfunction as a consequence of unresolved hyperglycaemia.[1] T2DM is a risk factor for the development of late onset Alzheimer's disease (LOAD).[2] Substantial evidence suggests that dysregulated insulin signalling may be a key early contributor to the development of LOAD.[3] Loss of insulin receptors (IRs) in brain microvasculature can alter the trafficking of insulin and its signalling in the brain.[4] Insulin signalling is critical for endothelial and neuronal function.[5] Alterations in insulin signalling are commonly observed in the brains of both type 2 diabetic and Alzheimer's disease patients.[6] Some studies suggest that the expression and activation of IR, insulin growth factor 1 receptor (IGF-1R) and insulin receptor substrate 1 (IRS-1) are reduced in the brains of Alzheimer's disease patients compared to healthy individuals[7] and that cortical levels of insulin and its binding to IRs are reduced in Alzheimer's disease patients.[8] Finally, a lower concentration of insulin in the CSF despite higher plasma insulin levels[9] suggests that there may be reduced insulin transport in the CNS of Alzheimer's disease patients. However, the molecular signals in type 2 diabetes that compromise insulin signalling in the brain and enhance the development of cognitive dysfunction and LOAD are not fully understood.[10-12]

Caveolin-1 (Cav-1) is the principal membrane protein of caveolae and is enriched in endothelial cells (ECs) in the periphery and cerebrovasculature.[13,14] Cav-1 depletion has been extensively implicated in the pathogenesis of type 2 diabetes.[15] Importantly, Cav-1 knock-out mice develop insulin resistance.[16] Cav-1 regulates insulin uptake and levels of IRs in adipocytes[17] and lung ECs.[18] We have shown that the expression of Cav-1 is altered in the brains of type 2 diabetes mouse models, thereby promoting the amyloidogenic pathway.[13] Here, we show that the levels of Cav-1 in brain endothelial cells (bECs) are significantly reduced in *db/db* mice. This reduction correlated with loss of IRs in the brain microvasculature. Furthermore, impairments associated with insulin signalling were observed in the parenchyma. Similar impairments, e.g. reduced expression of IRs in brain microvessels and alteration in insulin signalling in brain parenchyma, were observed in endothelial-specific *Cav-1*$^{-/-}$ (*Tie2Cre; Cav-1*$^{fl/fl}$) mice. This suggests that Cav-1 regulates IR levels and signalling, and that loss of endothelial Cav-1 is sufficient to promote IR depletion in the cerebrovasculature. We further demonstrate that Cav-1 in bECs is important for regulating insulin uptake and signalling. We show that IR directly interacts with Cav-1 and caveolae-associated proteins, Zonula Occludence-1 (ZO-1) and insulin-degrading enzyme (IDE). In addition, Cav-1 and IR co-localized in lipid rafts in the plasma membrane. Importantly, reconstitution of Cav-1 expression restored raft IR localization and insulin signalling in *Cav-1*$^{-/-}$ ECs. Taken together, these studies suggest that endothelial Cav-1 expression plays a critical role in maintaining insulin signalling in the brain.

Materials and methods

Animals

All animal procedures were approved by the University of Illinois at Chicago animal care and use committee. *Tie-2cre*$^{+}$*; Cav-1*$^{lox/lox}$ (EC-*Cav-1*$^{-/-}$) and *Cav-1*$^{-/-}$ mice were described previously.[19] Cre-negative littermates (*Tie-2Cre*$^{-}$*; Cav-1*$^{lox/lox}$) and C576Bl/6J were used as wild-type (WT) controls for EC-specific and global *Cav-1*$^{-/-}$ mice, respectively. Eight-week-old *db/db* mice were obtained from Jackson laboratory (*BKS.Cd-DOCK7*^{m}*+/+ Lep*$^{db/J}$, stock #000642).

Brain microvessel isolation

Brain microvessels were isolated as previously described.[10,20] *db/db* obesity-induced type 2 diabetic mice were sacrificed at 12 weeks of age, whereas EC-*Cav-1*$^{-/-}$ mice were used at 6 months of age. Briefly, mice were perfused with ice-cold phosphate-biffered saline (PBS) and the meninges and white matter were removed from the cortex under the microscope. The cortex was then minced using a stainless-steel blade and further homogenized using a glass dounce homogenizer. The homogenate was then mixed with equal volume of 30% dextran (70 kDa) to achieve a final concentration of 15%. The homogenate was then centrifuged at 6000*g* for 15 min at 4°C. The microvessel depleted fraction was on top of the dextran, whereas the microvessels were at the bottom of the microfuge tube. The microvessel-depleted fraction was then collected into a separate tube and washed five times to remove any trace of dextran. The microvessel pellet was further filtered through 70 mm and 40 μm filters to retain only capillaries. Both the capillary and depleted fractions were then further processed for western blotting as described below. Specific details on the reagents and the antibodies used can be found in the Supplementary material.

Endothelial cell culture

Brain endothelial cells were isolated from 1-month-old WT and *Cav-1*$^{-/-}$ mice as described previously.[21,22] The detailed methodology can be found in the Supplementary material.

Insulin signalling

Primary bECs from 1-month-old WT and *Cav-1*$^{-/-}$ mice were cultured in serum- and growth factor-free DMEM media for 4 h. Insulin was added at a concentration of 100 nM and incubated for 30 min. The media was removed, and the cells were washed twice with Hank's balanced salt solution containing calcium and magnesium. The cells were then collected using a cell scraper in RIPA buffer containing proteinase and phosphatase inhibitors. The cells were sonicated at 20% amplitude for 15 s. The lysate was centrifuged at 16 000*g* at 4°C and the supernatant was further used for western blot analysis.

Fluorescein isothiocyanate labelled-insulin uptake

The fluorescein isothiocyanate labelled (FITC)-insulin experiment was carried out as previously described.[23,18] Briefly, primary bECs from WT and *Cav-1*$^{-/-}$ mice were cultured on coverslips coated with collagen. After reaching confluence, cells were cultured in serum- and growth factor-free media for 1 h. The cells were then treated with 50 nM FITC-insulin. Five minutes later, the media was removed, and the cells were rinsed with acid wash buffer (acetic acid pH 2.5) to remove surface-bound insulin. The wash buffer was gently pipetted on the coverslip and removed without disturbing the cells on coverslip. The cells were then washed with PBS three

times for 5 min each followed by fixation with 4% paraformaldehyde (PFA). Cells were treated with DAPI for 5 min to label the nucleus, mounted on slides and imaged with a Zeiss LSM 710 confocal microscope. The groups were blinded for experimental analysis. FITC-insulin puncta were quantified using ImageJ analysis software as previously described.[18] Briefly, images were converted to 16-bit, greyscale format. Image threshold values were set to 50 or greater. For particle analysis, objects of 2–50 pixel units in size with circularity between 0.5 and 1.0 were counted. Within each replicate, the number of puncta per cell was quantified, then averaged across all replicates for each group.

Gold insulin preparation

Preparation of gold-conjugated insulin (Au–insulin) was carried out as previously described.[24-26] Briefly, a reduction mixture containing 1% sodium citrate, 1% tannic acid and 25 mM potassium carbonate was made in a Sigma coat-treated flask. The reduction mixture and 0.01% gold chloride solution were heated separately on the heating plate with gentle stirring. Once the temperature of solutions reached 60°C, both solutions were mixed. The mixture was then boiled for 20 min to completely reduce the gold. Once the gold solution cooled completely, it was stored at 4°C until further use. The concentration of insulin needed to stabilize the gold particles was identified by titration of different concentrations with same amount of gold solution. Insulin at 0.3 mg/ml optimally stabilized the gold solution. Furthermore, 1% glutamate was used to stabilize the Au–insulin complex. The solution was then centrifuged at 35 000 RPM for 1 h and stopped without applying any brake. The pellet containing Au–insulin particles was collected and stored at 4°C for further use. Concentration of Au–insulin complex was determined by absorbance at 520 nm.

Electron microscopy

In vitro insulin uptake

Cell monolayers cultured on Transwell filter inserts (Corning, 0.4 μm polyester filter) were treated with Au–insulin. After incubating for 30 min, the cells were fixed in cacodylate buffered (pH 7.2) solution of 2.5% glutaraldehyde, washed in 0.1 M cacodylate buffer (pH 7.2) and post-fixed in buffered 1% osmium tetroxide (pH 7.2) for 1 h. Dehydration was carried out by following the same steps as mentioned above. The cells were infiltrated with a mixture of LX-112 resin and ethanol (1:3, 1:1, 3:1 ratio for 30 min each) and overnight in 100% resin. Samples were placed in a 60°C oven to polymerize (3 days). Ultra-thin sections (~70 nm) were cut perpendicular to the Transwell membrane, collected onto 200-mesh copper–rhodium grids and contrasted with uranyl acetate and Reynold's lead citrate stains, respectively. Samples were observed with a JEOL JEM-1400F transmission electron microscope operating at 80 kV. Digital micrographs were acquired using an AMT Biosprint 12M-B CCD camera and AMT software.

Tissue imaging

Mice were perfused with PBS followed by a mixture of 2% PFA, 2% glutaraldehyde and 0.1 M cacodylate buffer. The brain was removed and fixed in 4% PFA containing 1% glutaraldehyde. The fixed brains were further sectioned with a vibratome at 80 μm thickness. Brain slices were washed in 0.1 M phosphate buffer (pH 7.2) and post-fixed in buffered 1% osmium tetroxide for 1 h. After several buffer washes, samples were dehydrated in an ascending concentration of ethanol (50%, 70%, 90%, 95%) leading to 100% absolute ethanol, followed by two changes in propylene oxide (PO) transition fluid. Specimens were infiltrated overnight in a 1:1 mixture of PO and LX-112 epoxy resin, and for 2 h in 100% pure LX-112 resin. Brain slices were flat embedded between two Aclar plastic films in normal BEEM capsules. The samples were cured at 60°C for 3 days. Ultra-thin sections (~70 nm) were cut (using a Leica Ultracut UCT model ultramicrotome), collected onto 200-mesh copper–rhodium grids, and contrasted with uranyl acetate and Reynold's lead citrate stains, respectively. Specimens were examined via JEOL JEM-1400F transmission electron microscope operating at 80 kV. Digital micrographs were acquired using an AMT Biosprint 12M-B CCD Camera and AMT software. All the reagents were electron microscopy grade and their details can be found in the Supplementary material.

Lipid raft isolation

Membrane lipid rafts were isolated as previously described.[27,28] Cells were cultured in T-75 flasks. At confluence, cells were collected in a 500 mM sodium bicarbonate buffer (pH 11) containing proteinase and phosphatase inhibitors. Cells were homogenized by a grinder and sonicated for 15 s at 20% amplitude and centrifuged at 1000 RPM for 10 min to separate any larger particles. The volume was further adjusted to 2 ml and mixed with 2 ml 90% sucrose made in 0.025 M MES [2-(*N*-morpholino) ethanesulfonic acid] and 0.15 M sodium carbonate [modified Barth's saline (MBS) buffer pH 6.5]. The resulting 45% sucrose was then layered with 4 ml of 35% sucrose and 4 ml of 5% sucrose made in MBS buffer. Gradients were centrifuged in a Beckman ultracentrifuge at 39 000 RPM for 16 h at 4°C using SW-41 rotor. One millilitre of each fraction was collected in separate Eppendorf tubes for processing by western blot as described above. The membrane lipid raft blots were analysed by calculating the percentage of target protein in each fraction.

Immunoprecipitation

Cells were lysed in a 1× cell lysis buffer containing phenylmethylsulfonyl fluoride (PMSF). The lysate was then sonicated for 15 s at 20% amplitude followed by centrifugation at 16 000*g* for 15 min. A portion of the supernatant was separated to be used as no immunoprecipitate control (~10%) and the remaining was divided into two equal parts; one for immunoprecipitation (IP) by anti-IR-β IgG and the other for pull down by isotype control IgG. The lysate was precleared with agarose G beads. The pre-cleared lysate was then further incubated overnight at 4°C with respective antibodies at 1:25 dilution. The agarose G beads were then added to the lysate and further incubated for 2 h in 4°C. Following incubation, the lysate was centrifuged at 4000 RPM for 5 min and the pellet was collected for further washing. The pellet containing agarose beads was then washed five times with the lysis buffer to remove any non-specific binding. The gel loading dye and sample buffer was added to the pellet and incubated at 95°C for 10 min to dissociate the complex. The sample to be loaded in the sodium dodecyl sulphate–polyacrylamide gel electrophoresis (SDS-PAGE) was separated from the beads by centrifuging at 14 000 RPM for 10 min. The samples were then run on the SDS-PAGE as described above. To distinguish between the IgG light chain and Cav-1, Veriblot IP detection reagent was used. This reagent specifically detects the native primary antibody further avoiding detection of heavy and light chain fragments generated during IP.

Transduction in cell culture

Gene transduction in the primary bECs was carried out as previously described.[29] In short, for the analysis of IRs and signalling, cells were cultured in six-well plates and treated with 2.5×10^{10} viral genome/well on Day 3 after isolation. For the lipid raft extractions, the cells were cultured on T-25 flasks with 3.5×10^{10} viral genome/flask. The virus-containing media was removed 3 days after the treatment and the cells were cultured until they reached confluence. The cells were then collected for appropriate assays as described above.

Co-immunoprecipitation for proteomics

Immunoprecipitation of IR-β from *Cav-1*$^{-/-}$ and WT cells using IR-β antibody was performed with a Pierce Co-IP Kit (ThermoFisher Scientific). In brief, cell pellets were lysed in IP lysis/wash buffer (provided in the kit) containing Pierce protease inhibitor cocktail (ThermoFisher Scientific). Protein concentration was determined using the bicinchoninic acid (BCA) assay. To immobilize the antibody onto the spin column with AminoLink Plus Coupling Resin, 10 μg of IR-β antibody was prepared in 1× coupling buffer and loaded onto the spin column. One milligram of protein lysate from each sample was pre-cleared following the manufacturer's instructions, and the flowthrough was loaded onto the IP column immobilized with the antibody. Incubation was performed by end-to-end rotation at 4°C overnight. The next day, unbound proteins were removed by centrifugation and the resin-bound proteins were washed three times with IP lysis/wash buffer. Resin-bound proteins were then eluted using the elution buffer provided in the kit, and eluents were used for digestion and further analysis by mass spectrometry.

Protein digestion

Proteins eluted from co-immunoprecipitation (Co-IP) or whole-cell lysates were reduced with 20 mM dithiothreitol at 95°C for 10 min, followed by alkylation with 40 mM iodoacetamide at room temperature in the dark for 30 min. Proteins were then acidified by phosphoric acid and loaded onto the S-trap Micro Spin Column (Protifi). After multiple washes with the S-trap binding buffer [90% MeOH, 100 mM of triethylammonium bicarbonate (TEAB)], 1 μg of trypsin in 50 mM TEAB was then added onto the column and incubated at 37°C overnight. Digested peptides were eluted with each of the following solutions: 50 mM TEAB, 0.1% formic acid (FA) and 50% acetonitrile with 0.1% FA, and combined. The peptides were dried down prior to resuspension in 0.1% FA for liquid chromatography–mass spectrometry (LC-MS) analysis.

Liquid chromatography–mass spectrometry analysis

Resuspended peptides were injected into a Thermo NanoViper trap column (75 μm × 20 mm, 3 μm C18, 100 Å; Thermo Fisher Scientific) installed on an Agilent 1260 Infinity nanoLC system (Agilent Technologies) and washed for 10 min with 0.1% FA at 2 μl/min flowrate. Peptides were eluted with a 120-min gradient [from 5% to 60% acetonitrile (ACN) with 0.1% FA], at 250 nl/min flowrate, on an Agilent Zorbax 300SB-C18 column (75 μm × 150 mm, 3.5 μm, 300 Å), where mobile phase A was 0.1% FA and mobile phase B was 0.1% FA in ACN. Data collection was done using data-dependent acquisition analysis by a Thermo Q Exactive mass spectrometer (Thermo Fisher Scientific). MS/MS was performed using high-energy collision dissociation for the top 10 precursors. Settings for the mass spectrometer were as follows: capillary temperature at 250°C, spray voltage 1.5 kV, MS1 scan at 70 000 resolution, scan range from 375 to 2000 *m*/*z*, automatic gain control target 1×10^6 for a maximum injection time of 100 ms. The isolation width was set at 1.2 *m*/*z* and dynamic active exclusion set for 20 s. MS/MS spectra were collected at 17 500 resolution, for a maximum injection time of 50 ms with a minimum of 1×10^5 ions. Normalized collision energy was set to 27%. Masses with charges of 1 and larger than 6 were excluded from the MS/MS analysis. All raw MS data are deposited in the MassIVE repository under dataset identifier id: MSV000091296.

Protein identification

Raw files from the LC-MS analysis were imported into Proteome Discoverer 2.2 (Thermo Fisher Scientific) using the Sequest HT search engine against the UniProt *Mus musculus* database (downloaded on 27 April 2017). Trypsin was set as the protease with two missed cleavages with sequence lengths between 6 and 144 amino acids. Precursor and fragment mass error tolerances were set to 10 ppm and 0.02 Da, respectively. Peptide dynamic modifications allowed during the search were oxidation (M), deamination (N, Q), and acetylation (N-terminus), whereas carbamidomethyl (C) was set as static modifications. Protein identifications are provided in Supplementary Tables 1 and 2.

Statistical analysis

Statistical analysis was performed by using GraphPad Prism (Version 9) software. Western blots were analysed using densitometry and compared by unpaired two-tailed *t*-test or one-way ANOVA. A probability of <0.05 is considered statistically significant and the data ar presented as mean ± SEM. Statistical analysis performed for individual figures is described in figure legends.

Data availability

The data that support the findings of this study are available on request from the corresponding author.

Results

Altered brain Cav-1 expression correlates with impaired insulin signalling in *db/db* mice

We have shown previously that levels of Cav-1 were reduced in the brains of *db/db* mice.[13] However, while Cav-1 is enriched in ECs, it is also expressed in neurons and glia. Thus, we examined whether these alterations take place in the cerebrovasculature. For that, we utilized dextran-mediated separation of brain capillaries from non-vascular tissues.[30] These microvessels were enriched with endothelial nitric oxide synthase (eNOS) as well as Cav-1 (Supplementary Fig. 1). We observed that levels of Cav-1 were significantly reduced in microvessels of *db/db* compared to age-matched WT mice (Fig. 1A and B). In addition, levels of IR-α and -β were reduced in these microvessels (Fig. 1A, C and D). As IRs are critical in promoting insulin signalling, we examined the expression of the downstream signalling intermediate, Akt, which is phosphorylated by IR following insulin binding–induced IR activation.[31] Phosphorylated Akt (p-AktSer473) was reduced in the microvessels of *db/db* mice, while total levels of Akt remained unchanged. This suggests chronic impairment of insulin signalling in the microvessels of *db/db* mice (Fig. 1E–G). In addition, as

phosphorylation of Cav-1 at Tyr14 is essential for the trafficking of solutes across brain blood vessels,[32] we examined the levels of phosphorylated Cav-1 (p-Cav-1Tyr14) in the microvessels. Levels of p-Cav-1Tyr14 were significantly reduced in *db/db* microvessles compared to brain microvessels of WT (Fig. 1E, H and I), but the ratio of p-Tyr14-Cav-1/total Cav-1 was unaltered, suggesting that reduced p-Cav-1Tyr14 level may result from reduced total Cav-1 rather than reduced Src kinase activity.

Next, we examined whether expression of Cav-1 is altered in the parenchyma of *db/db* mice. In contrast to the microvessel fraction, there was a significant elevation in the level of Cav-1 (Fig. 1J and K). As the microvessel-depleted parenchymal fraction contains an extremely low level of Cav-1 compared to the microvessel fraction (Supplementary Fig. 1A), we hypothesized that multi-fold increase in Cav-1 in the *db/db* microvessel-depleted fraction might be due to inflammation-induced vesicular shedding from ECs, which has been shown to be a mechanism for Cav-1 loss from the vasculature.[19] To examine this, we probed the microvessel-depleted fraction with antibodies raised against Annexin-V, a proxy of extracellular vesicles (EVs).[33] We observed Annexin-V to be upregulated in the *db/db*-depleted fraction, as compared to that from WT mouse brains, indicating accumulation of EVs (Supplementary Fig. 2A). In addition, we further corroborated our findings by Nanosight microparticle analysis of the depleted fractions. EV size distribution and their total number were both elevated in the *db/db* mouse brain microvessel-depleted fraction (Supplementary Fig. 2B). Overall, these results show that alterations in the level of Cav-1 in the microvessels of *db/db* mice correlated with impaired levels of IRs and downstream signalling. In addition, alterations in endothelial Cav-1 expression have implications for its levels in the parenchyma. Thus, we examined levels of parenchymal IRs in the microvessel-depleted fractions extracted from the brains of WT and *db/db* mice. IR-α was significantly upregulated in the parenchyma of *db/db* mice compared to the WT, whereas level of IR-β was unchanged (Fig. 1J, L and M).

Endothelial cell-specific Cav-1 knock-out impairs brain insulin signalling in vascular and non-vascular cells

To investigate if the loss of Cav-1 in ECs could cause impairments in insulin signalling in the brains of *db/db* mice, we utilized EC-specific Cav-1 knock-out mice (*Tie2Cre*; *Cav-1*$^{fl/fl}$; EC-*Cav-1*$^{-/-}$). Similar to *db/db* brains, a significant reduction in the levels of the IR-α and -β was observed in microvessels isolated from the brains of EC-*Cav-1*$^{-/-}$ mice (Fig. 2A–C). In addition, phosphorylation of Akt was significantly reduced in the microvessels of EC-*Cav-1*$^{-/-}$ mice (Fig. 2D–F). These microvessels were enriched with endothelial markers, such as eNOS and VE-Cadherin (Supplementary Fig. 1C and D). We then asked if EC deletion of Cav-1 had a non-autonomous role in regulating insulin signalling outside the vasculature, for example in the brain parenchymal fraction. We observed that levels of Cav-1 were similar in the parenchymal fraction of EC-*Cav-1*$^{-/-}$ and WT mice (Fig. 2G and H). This supported our speculation that the increase in Cav-1 in the parenchymal fraction of *db/db* mice was not directly due to lack of endothelial Cav-1 (Fig. 1J and K). Furthermore, the level of IR-α was decreased in EC-*Cav-1*$^{-/-}$, whereas the level of IR-β was increased (Fig. 2G–J), suggesting alterations in the expression and stoichiometry of IRs. We next examined whether this may result in the disruption of insulin signalling within the parenchymal fraction. Interestingly, deletion of Cav-1 in the vasculature caused reduced levels of p-Cav-1(Y14), Akt (S473) and glycogen synthase kinase-3β (Y216) [p-GSK-3β (Y216)] in the depleted fraction, with no change in the total levels of these proteins (Fig. 2K–Q). GSK-3β is involved in phosphorylation of cytoskeletal proteins in neurons.[34] The phosphorylation of GSK-3β at Y216 is important for its constitutively active form.[34] Insulin signalling inactivates GSK-3β by Akt-mediated phosphorylation at the serine 9 (S9) residue.[35] Interestingly, there was a trending increase in levels of the inactive form GSK-3β-S9, albeit not statistically significant (Fig. 2K and Q). Overall, these results suggest that lack of Cav-1 in ECs affects insulin signalling not only in the vasculature but also in neurons and glia.

Cav-1 is essential for insulin uptake in brain endothelial cells

To examine whether insulin uptake in endothelial cells is Cav-1–dependent, we isolated bECs from WT and *Cav-1*$^{-/-}$ mice. We first validated that the phenotype of bECs derived from *Cav-1*$^{-/-}$ resembles our findings in *db/db* and EC-*Cav-1*$^{-/-}$ microvessels. Indeed, the levels of IR-α and -β were significantly lower in bECs isolated from *Cav-1*$^{-/-}$ mice (Fig. 3A–C). To examine whether lack of Cav-1 compromises insulin uptake, bECs were treated with insulin. A significant reduction in the phosphorylation of Akt was observed in *Cav-1*$^{-/-}$ ECs following insulin treatment compared to insulin-treated WT bECs (Fig. 3D–F), suggesting that insulin uptake may be compromised.[36] To further address this, we treated bECs isolated from WT and *Cav-1*$^{-/-}$ mice with FITC-insulin. *Cav-1*$^{-/-}$ bECs exhibited reduced uptake of FITC-insulin compared to WT (Fig. 3G and H). As FITC-insulin is not detectable by confocal microscope at low concentration (Supplementary Fig. 3), we treated the bECs with 50 nM FITC-insulin. Furthermore, immunolabelling of Cav-1 in FITC-insulin–treated WT bECs showed significant co-localization, suggesting caveolae-mediated insulin uptake (Fig. 3I). In addition, FITC-insulin co-localized with Rab5, an early endosomal proxy, suggesting that the route of insulin trafficking in ECs is via the endosomal sorting pathway (Fig. 3J). *Cav-1*$^{-/-}$ bECs showed reduced insulin uptake and co-immunolabelling and did not show presence of insulin in early endosomes (Supplementary Fig. 4). To validate that insulin uptake is receptor-mediated we performed competitive ligand and receptor desensitization assay. For competitive ligand assay, we added a 10-fold greater amount of unlabelled insulin with FITC-insulin. In the receptor desensitization assay, we treated the cells with unlabelled insulin for an hour and then treated with FITC-insulin. In both cases we observed reduced uptake by bECs (Supplementary Fig. 5). Taken together, these results suggest that insulin uptake is receptor-dependent. To achieve the spatial resolution required for assessment of FITC-insulin internalization, we utilized electron microscopy to visualize Au–insulin uptake by bECs. Insulin internalization was readily detectable in the WT bECs. Insulin was taken up by endocytic vesicles resembling caveolae in the WT bECs (Fig. 3K). Interestingly, insulin uptake was undetectable in *Cav-1*$^{-/-}$ ECs. Instead, insulin was found on the plasma membrane of these cells (Fig. 3K). Taken together, these experiments suggest that insulin uptake in ECs is Cav-1-dependent and is mediated by caveolae.

Cav-1 knockout destabilizes the spatial localization of insulin receptors in the cell membrane

Cav-1 has been implicated in several signalling pathways by regulating the localization of receptors in caveolae/lipid rafts in the plasma membrane.[37] To determine if Cav-1 regulates insulin

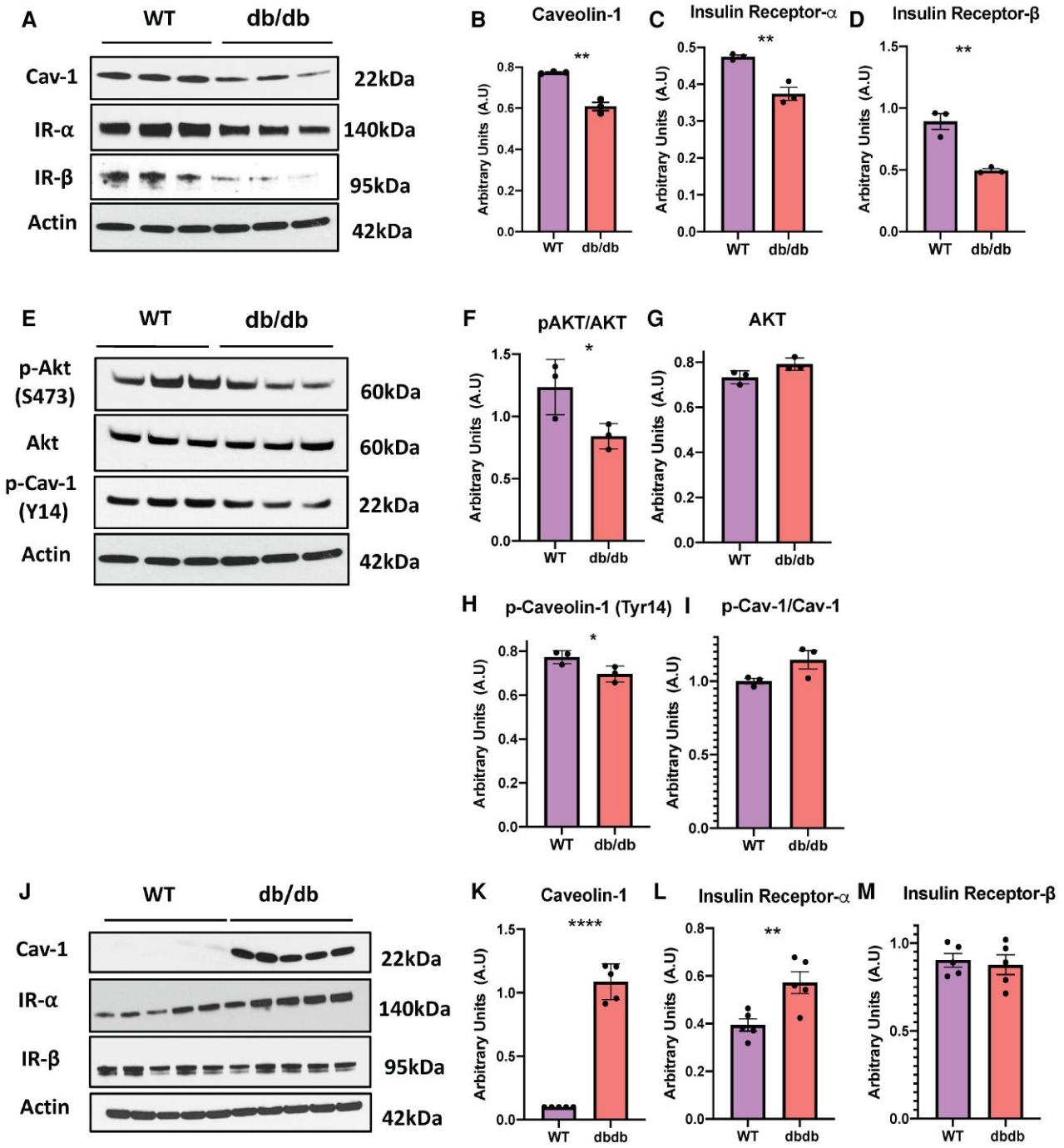

Figure 1 Impaired IR expression and activation in the brain of *db/db* mice. (**A–I**) Expression of Cav-1, IR-α and IR-β (**A**), p-Akt(S473), Akt and p-Cav-1 (**E**) in brain microvessels of WT and *db/db* mice as detected by western blot analysis. The phospho and total protein levels were examined in the same samples. (**B–D** and **F–I**) Quantification of expression levels of Cav-1 (**B**), IR-α (**C**), IR-β (**D**), p-Akt(S473)/Akt (**F**), Akt (**G**), p-Cav-1 (Y14) (**H**) and p-Cav-1/Cav-1 (**I**) in brain microvessel fractions. (**J–M**) Expression of Cav-1, IR-α and IR-β in brain microvessel–depleted fractions from WT and *db/db* mice by western blot analysis. (**K–M**) Quantitative analysis of Cav-1 (**K**), IR-α (**L**) and IR-β (**M**). ($n = 6$ for microvessels, Each replicate represents pooled microvessels from two animals. $n = 5$ for microvessel-depleted fraction, unpaired *t*-test, $^{*}P < 0.05$, $^{**}P < 0.01$.)

signalling via modulation of receptor localization in lipid rafts in ECs, we utilized sucrose gradient ultracentrifugation[28] for lipid raft extraction from bECs bEnD3. We observed the presence of Cav-1 in the lipid raft fractions (fraction 4–6, Fig. 4A) and IR-α (agonist binding subunit) specifically localized to the same fractions. The majority of IR-β (cytosolic catalytic subunit) was detected in lipid raft fractions but was also present in non-lipid raft fractions (Fig. 4A). Given that a functional IR is formed by the interaction of IR-α and IR-β,[38,39] it would be reasonable to assume that this interaction takes place in lipid rafts, whereas upon IR-β activation, signal transduction ensues in the non-lipid raft zones. In support of this notion, Akt, known to localize to the cytosol, was observed within the non-lipid raft fraction (Fig. 4A).

The mechanism of IR endocytosis has not been fully elucidated and is speculated to be cell-type specific.[39] In adipocytes, both clathrin- and caveolae-mediated endocytosis of IR has been

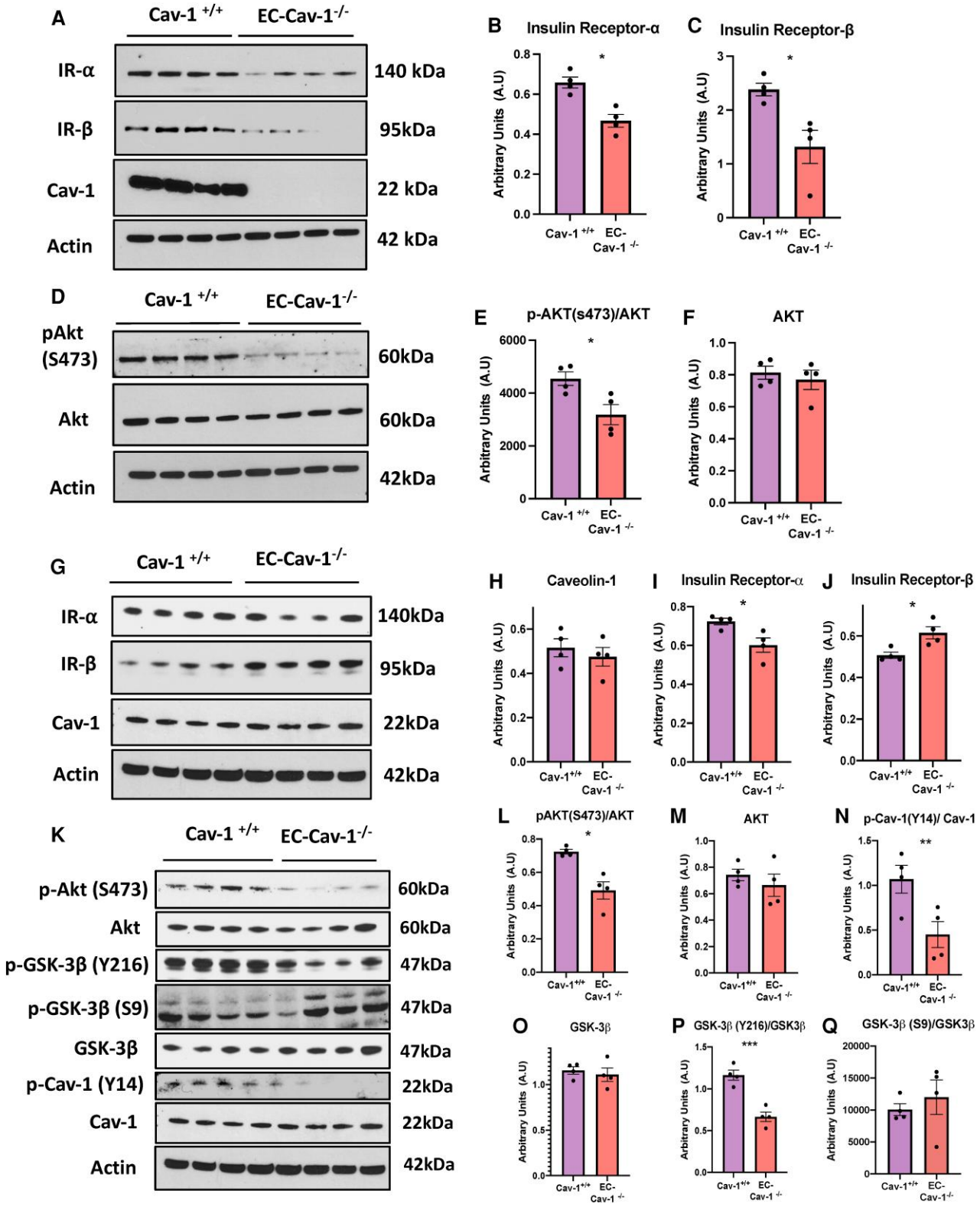

Figure 2 Endothelial-specific Cav-1 knock-out mice exhibit impaired insulin signalling. (**A**) Western blot analysis of IR-α, IR-β and Cav-1 protein expression in brain microvessels of *Cav-1*$^{+/+}$ and EC-*Cav-1*$^{-/-}$ mice. (**B** and **C**) Quantitative analysis of IR-α and IR-β in *Cav-1*$^{+/+}$ and EC-*Cav-1*$^{-/-}$ mice. (**D**) Western blot analysis of p-Akt(S473) and Akt protein levels in brain microvessels of *Cav-1*$^{+/+}$ and EC-*Cav-1*$^{-/-}$ mice. (**E** and **F**) Quantitative analysis of p-Akt (S473) and Akt. (**G**) Western blot analysis of Cav-1, IR-α and IR-β protein levels in brain microvessel-depleted fraction of *Cav-1*$^{+/+}$ and EC-*Cav-1*$^{-/-}$ mice. (**H–J**) Quantitative analysis of IR-α and IR-β in brain microvessel-depleted fraction of *Cav-1*$^{+/+}$ and EC-*Cav-1*$^{-/-}$ mice. (**K**) Western blot analysis of protein levels of p-Akt (S473), p-GSK-3β(Y216), p-GSK-3β(S9), p-Cav-1(Y14) and total levels of Akt, GSK-3β and Cav-1 in brain microvessel–depleted fraction of *Cav-1*$^{+/+}$ and EC-*Cav-1*$^{-/-}$ mice. (**L–Q**) Quantification of p-Akt (S473) (**L**), total levels of Akt (**M**), p-Cav-1(Y14)/Cav-1 (**N**), GSK-3β (**O**), p-GSK-3β(Y216)/GSK-3β (**P**), p-GSK-3β(S9)/GSK-3β (**Q**) in brain microvessel–depleted fraction of *Cav-1*$^{+/+}$ and EC-*Cav-1*$^{-/-}$ mice. ($n = 5$, unpaired *t*-test, $^{*}P < 0.05$, $^{**}P < 0.01$, $^{***}P < 0.001$.)

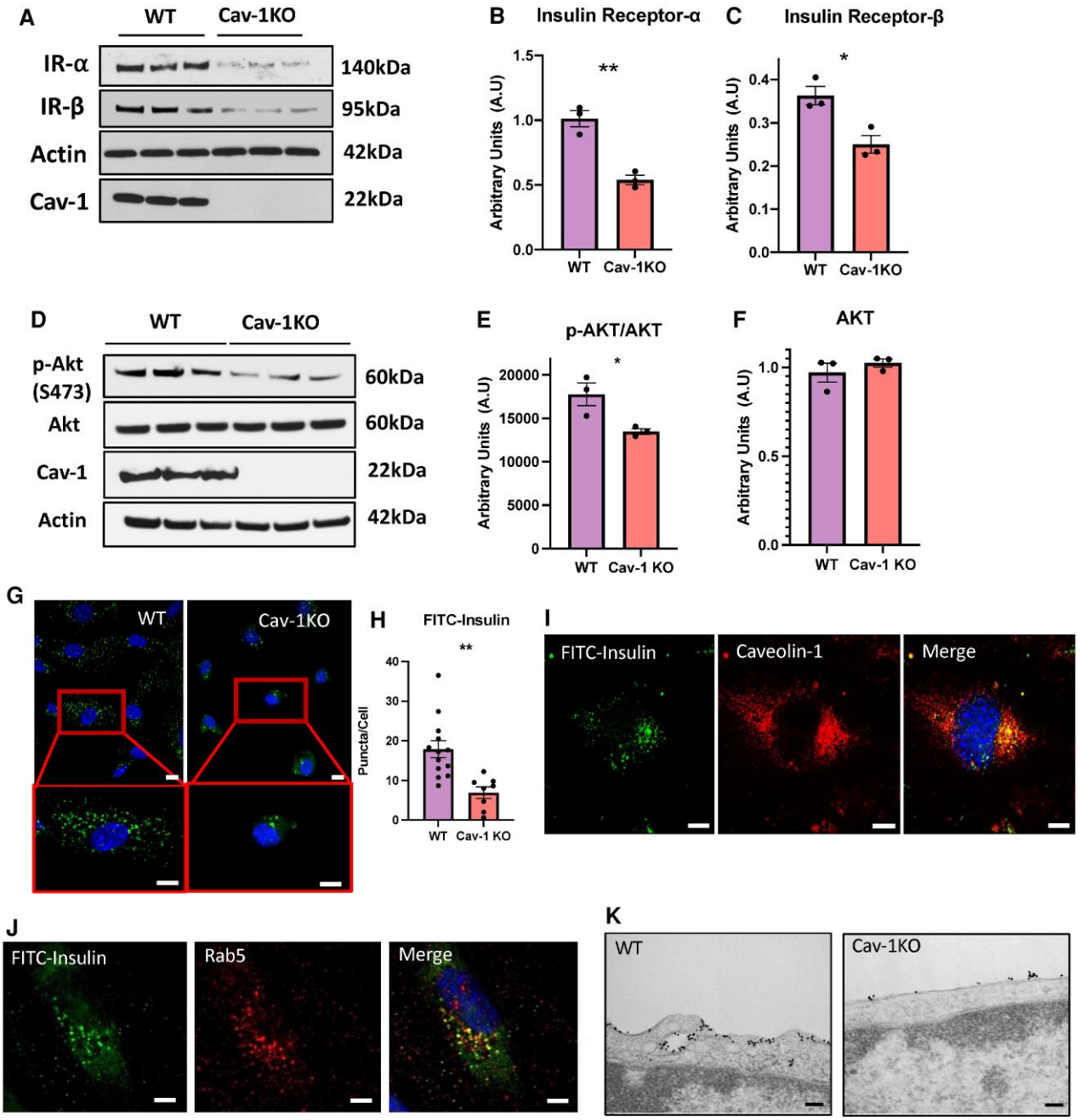

Figure 3 Insulin uptake and signalling is regulated by Cav-1. (**A**) Protein expression of IR-α, IR-β and Cav-1 in bECs as detected by western blot analysis. (**B** and **C**) Quantitative analysis of IR-α and IR-β in bECs. (**D**) Western blot analysis of protein expression of p-Akt (S473), Akt and Cav-1 in bECs following insulin stimulation. (**E** and **F**) Quantitative analysis of p-Akt and Akt in bECs. (**G**) Representative fluorescent images of FITC-insulin uptake in WT and *Cav-1*$^{-/-}$ bECs. Scale Bar = 20 μm (**H**) Quantification of FITC-insulin uptake in brain endothelial cells isolated from WT and *Cav-1*$^{-/-}$. (**I**) Representative images of co-immunolabelling of FITC-insulin and Cav-1 in WT bECs. Scale Bar = 10 μm (**J**) Co-immunolabelling of Rab-5 and FITC-insulin in WT bECs. Scale Bar = 10 μm. (**K**) Electron microscopy images of Au–insulin uptake and surface labelling of WT and *Cav-1*$^{-/-}$ bECs. Scale bars = 100 nm ($n = 3$, unpaired *t*-test, $^{*}P < 0.05$, $^{**}P < 0.01$).

described.[17,40-44] Thus, we examined the expression of clathrin in the membrane fractions. As expected, clathrin was present in the non–lipid raft fractions (Fig. 4A). In light of these results we asked whether Cav-1 directly interacts with IR. Cav-1 contains a scaffolding domain by which it interacts with signalling receptors,[37] and thus we hypothesized that it can interact with IR-β via this domain. To examine this, we immunoprecipitated IR-β from bEnD3 cells using anti-IR-β antibodies and examined the presence of Cav-1 in the immunoprecipitated fraction. The results showed the expression of Cav-1 in the IR-β–enriched fraction (Fig. 4B), suggesting that Cav-1 may directly interact with IR-β, which may be important for the stabilization of IR-β in lipid rafts. To further address this, we examined the implications of the lack of EC-Cav-1 expression on the membrane localization of IRs. For this, we isolated membrane lipid rafts from the WT and *Cav-1*$^{-/-}$ bECs and quantified the relative abundance of IR-β in the lipid rafts versus non-lipid raft fractions. We observed a significant decrease in the presence of IR-β in the lipid raft fractions of *Cav-1*$^{-/-}$ bECs compared to lipid rafts from WT bECs

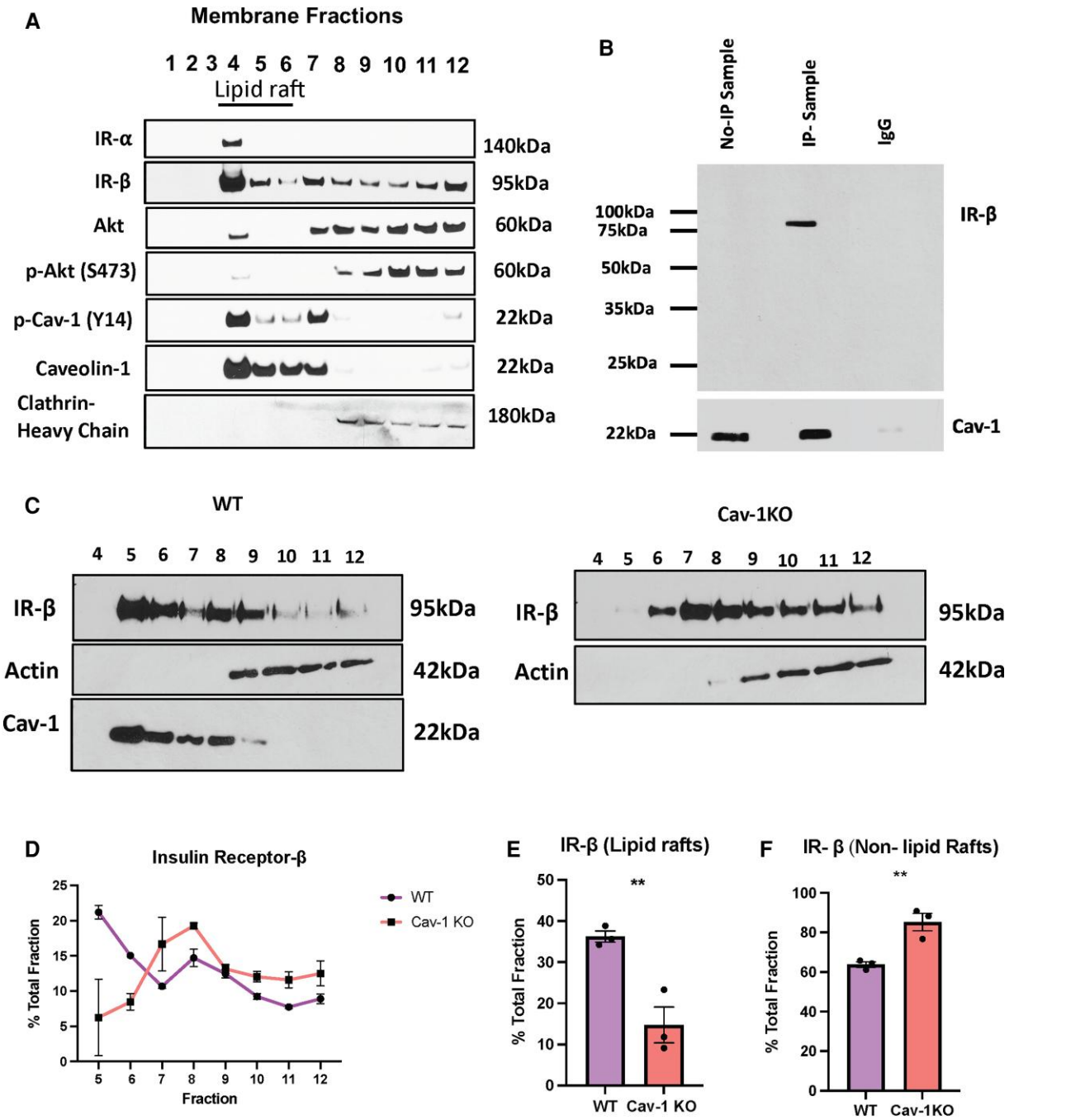

Figure 4 Cav-1 regulates localization of insulin receptors in membrane lipid rafts. (**A**) Expression of IR-α, IR-β and Cav-1, p-Akt (S473) and Akt in membrane fractions of bEnD3 bECs. (**B**) Co-immunoprecipitation of Cav-1 with IR-β Ab from bEnD3. Immunoprecipitation was repeated with isotype IgG control. (**C**) Localization of IR-β and actin in membrane fractions from WT (*left*) and *Cav-1*$^{-/-}$ (*right*). (**D–F**) Quantitative analysis of protein levels of IR-β in different membrane fractions isolated from WT and *Cav-1*$^{-/-}$ bECs ($n = 3$, unpaired *t*-test, $^{*}P < 0.05$, $^{**}P < 0.01$).

(Fig. 4C and E). In addition, the IR-β levels were increased in the non-lipid raft fractions of the *Cav-1*$^{-/-}$ bECs compared to WT bECs (Fig. 4C and F), overall suggesting alterations in the localization of IR-β within the plasma membrane of *Cav-1*$^{-/-}$ bECs. To evaluate whether loss of Cav-1 affects the localization of receptors known to be internalized *via* clathrin-mediated endocytosis, we examined the membrane localization of transferrin receptor. We observed that transferrin receptor was present in non-lipid raft fractions of both WT and Cav-1 knock-out bECs and co-localized with fractions enriched in clathrin heavy chain (Supplementary Fig. 6A and B, respectively). Taken together, these results suggest that Cav-1 plays an important role in the spatial stabilization of IR-β in lipid rafts containing IR-α in the cerebrovasculature.

The insulin receptor interactome in endothelial cells reveals linkages between Cav-1 and T2DM

Based upon our observations of Cav-1 contributing to insulin uptake and the loss of Cav-1 disrupting the distribution of the IR, we sought to gain insight into the protein network of the IR in ECs. To this end,

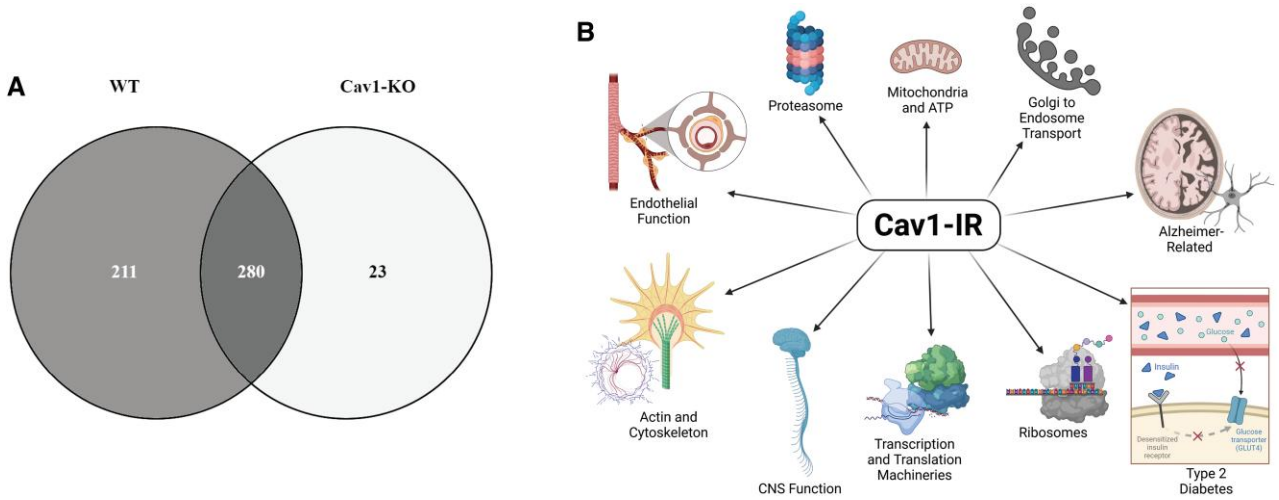

Figure 5 Immunoprecipitation of IR-β–associated protein complexes from bECs. (A) Venn diagram depicting the number of proteins identified in wild-type (light grey) and Cav-1 knock-out (white) cells that are interactors with the IR. The overlap of proteins interacting with the IR are depicted in dark grey (280 identifications). **(B)** Analysis of the 211 unique proteins of the IR interactome revealed functions associated with endothelium, the proteasome, mitochondria, Golgi to endosome transport, transcription and translational machinery, actin and cytoskeleton, CNS functions, the ribosome and associations with Alzheimer's disease and type 2 diabetes.

we performed co-immunoprecipitation in the presence and absence of Cav-1 (Fig. 5A) and found that while significant overlap was observed, 211 proteins were identified to interact with the IR in the presence of Cav-1. Further analysis of the unique protein list revealed proteins associated with critical cellular functions. Most notably, we observed those associated with CNS function, Alzheimer's disease and T2DM (Fig. 5B). Using the Reactome Pathway Browser tool, most specific pathways were obtained for the proteins that interact with the IR in the presence of Cav-1 (Table 1). Importantly, we considered crucial protein–protein interactions that would further shed light on the interaction of Cav-1 and IRs. Shown in Table 2, several caveolae-related proteins are observed to interact with the IR, including Cav-1, caveolae-associated proteins 1 and 2, IDE, Map1b, Creb1 and tight junction protein ZO-1. These results provide further evidence of the interaction between Cav-1 and the IR as well as insight into the potentially larger network of proteins crucial for insulin signalling.

Restoring Cav-1 in Cav-1 knock-out endothelial cells rescues insulin receptor expression and signalling

To assess causality of the loss of IRs, insulin uptake and signalling associated with depletion of EC-Cav-1, we asked whether reconstitution of Cav-1 expression would rescue the expression level of IRs. To address this, we developed an adeno-associated virus expressing Cav-1 (Supplementary Fig. 7). We first validated the efficacy of the virus by infecting *Cav-1*$^{-/-}$ bECs. We showed that restoring Cav-1 levels rescued the expression of IRs (Fig. 6A–C), as well as the phosphorylation of Akt following insulin treatment (Fig. 6D–F). In addition, the percentage of IR-β within lipid rafts was restored to that observed in WT lipid rafts (Fig. 6G–I). Taken together, these results suggest EC-Cav-1 plays a major role in the regulation of insulin uptake and signalling in bECs.

Discussion

In the brain parenchyma, insulin regulates Aβ production and reduced insulin signalling exacerbates amyloidosis.[45,46] Insulin has been implicated in regulation of genes involved in hippocampal neurotransmission,[47] synaptic function and learning and memory.[48] In turn, insulin resistance is linked to neuronal senescence and tau hyperphosphorylation in neurons, exacerbating neurodegeneration.[49,50] Neurofibrillary tangles and amyloidosis are the pathological hallmarks of Alzheimer's disease.[3] Hence, this study sought to examine the implications of altered endothelial Cav-1 expression on insulin trafficking and signalling in the brain.

In this study, we made several novel observations. First, we observed a reduction in the level of EC Cav-1 in cerebral microvessels of *db/db* type 2 diabetic mice. Second, we found that depletion of Cav-1 correlated with reduced expression of IR α and β subunits. Brain endothelial IRs regulate insulin signalling kinetics and trafficking within the brain. [4,36,51] As the brain primarily depends on peripheral insulin,[4] any alterations in EC expression of IRs and activation-dependent transcytosis into the brain can alter critical insulin signalling functions in the brain. We found that the depletion of endothelial Cav-1 in the cerebrovasculature of *db/db* mice affected insulin signalling in the parenchyma, as well as increased IR-α level, which may suggest a compensatory mechanism triggered by reduced availability of insulin. Cav-1 is thought to be depleted from the ECs by two mechanisms; one is the shedding of extracellular vesicles and the second is Cys156 nitrosation followed by Tyr14 phosphorylation and Lys86 ubiquitination resulting in its targeting for proteosomal degradation pathway.[19,52] Both pathways are initiated by a chronic state of inflammation and mainly driven by elevated levels of cytokines, such as TNF-α, TGF-β and IL-6.[19,53] Importantly, these cytokines were shown to cause endothelial dysfunction in *db/db* mice.[54] Taken together with our data, we rationalized that the primary mechanism of EC Cav-1 depletion is likely cytokine-induced shedding of Cav-1 positive EVs that accumulate in the parenchyma. As microvascular dysfunction can underline the changes occurring in brain parenchyma, we accessed the alterations associated with IRs and downstream signalling components in the microvessel-depleted brain parenchyma of EC-*Cav-1*$^{-/-}$ mice and observed reduced levels of IR-α and elevated IR-β in the EC-*Cav-1*$^{-/-}$ brain parenchyma. These observations suggest reduced insulin signalling in the extravascular brain tissue is

Table 1 Pathway analysis of EC IR interactors

Pathway	No. of entities	Total	Entities P-values
GTP hydrolysis and joining of the 60S ribosomal subunit	27	113	1.11×10^{-16}
Formation of a pool of free 40S subunits	24	102	1.11×10^{-16}
Nonsense-mediated decay	24	117	1.11×10^{-16}
Nonsense-mediated decay enhanced by the exon junction complex	24	117	1.11×10^{-16}
Cap-dependent translation initiation	28	120	1.11×10^{-16}
Eukaryotic translation initiation	28	120	1.11×10^{-16}
L13a-mediated translational silencing of ceruloplasmin expression	28	112	1.11×10^{-16}
Response of EIF2AK4 (GCN2) to amino acid deficiency	23	102	1.11×10^{-16}
Metabolism of RNA	49	679	1.11×10^{-16}
Regulation of expression of SLITs and ROBOs	35	172	1.11×10^{-16}
Cellular response to stress	60	765	1.11×10^{-16}
Axon guidance	45	558	1.11×10^{-16}
Cellular responses to stimuli	60	779	1.11×10^{-16}
Signalling by ROBO receptors	38	218	1.11×10^{-16}
Metabolism of amino acids and derivatives	39	375	1.11×10^{-16}
Nonsense-mediated decay independent of the exon junction complex	21	96	2.22×10^{-16}
Nervous system development	45	584	2.22×10^{-16}
Peptide chain elongation	20	90	7.77×10^{-16}
Eukaryotic translation termination	20	94	1.67×10^{-15}
Selenocysteine synthesis	20	94	1.67×10^{-15}

Table 2 IR interactors in relation to Cav-1 expression

Protein name	No. of peptides	Spectral matches
Insulin-degrading enzyme	15	20
Tight junction protein ZO-1	2	2
Microtubule-associated protein	2	2
Cyclic AMP-responsive element-binding protein-1	2	3
Caveolae-associated protein 1	6	12
Caveolae-associated protein 2	3	4
Cav-1	3	3

due to Cav-1 depletion in bECs. Our studies also showed reduced phosphorylation of the Akt and GSK-3β. Phosphorylation of Akt and GSK-3β are associated with neuronal survival signalling.[35] In addition, the phosphorylation of GSK-3β is essential for its activation and its role in the phosphorylation of cytoskeletal tau protein involved in neurodegenerative diseases.[55,56]

Previous studies have established the role of Cav-1 in regulating neuronal function.[57] We observed that endothelial deletion of Cav-1 did not have any effect on the levels of Cav-1 in non-vascular cells but rather on the phosphorylation of Cav-1 on Tyr14, which is critical for caveolae-mediated endocytosis and Cav-1 scaffolding functions,[32] suggesting altered neuronal function in the EC-*Cav-1*$^{-/-}$ mice. Interestingly, a significant elevation in the level of Cav-1 was observed in the parenchyma of the *db/db* but not EC-*Cav-1*$^{-/-}$ mice. This may suggest that the increase is not directly due to the lack of Cav-1 in ECs but rather release from ECs and accumulation in the surrounding tissue. One mechanism by which Cav-1 is removed from ECs is extracellular vesicle shedding, which is known to be triggered by inflammatory conditions and EC injury[19] associated with pulmonary arterial hypertension[19] and type 2 diabetes.[58] In this regard, Cav-1–enriched vesicles from ECs have been shown to impair the differentiation of neural stem and progenitor cells.[59]

Impairments in insulin signalling within ECs have been linked with vascular dysfunction such as atherosclerosis, aberrant angiogenesis and cardiomyopathy.[60,61] Insulin resistance or deficiency can induce these alterations by selectively preventing the activation of the PI3K/Akt pathway.[62] This pathway is essential for regulating the expression of vascular endothelial growth factor (VEGF) and eNOS.[63,64] These factors are involved in angiogenesis and vasodilation, respectively.[63,64] Previous studies have shown reduced VEGF and eNOS levels in the brains of *db/db* mice.[65,66] Here, we showed that *db/db* and endothelial-specific *Cav-1*$^{-/-}$ microvessels exhibit reduced IR levels and phosphorylation of Akt. Our studies revealed compromised phosphorylation of Akt in steady state, as well as following insulin stimulation in Cav-1–depleted ECs. Because IRs and phosphorylated Akt are upstream of VEGF expression and eNOS activation, this suggests depletion of endothelial Cav-1, resulting in reduced insulin signalling and associated microvascular dysfunction in *db/db* mice.

IR-mediated insulin signalling in bECs is important for insulin uptake (Supplementary Fig. 5).[36] Moreover, the presence of Cav-1 further supports a critical role of IR signalling based on evidence of the presence of caveolae-interacting proteins as well as IDE in the IR-β immunoprecipitated protein complex. The loss of serum IDE levels has been proposed as a risk factor for Alzheimer's disease in T2DM patients, although in small cohorts serum levels of IDE have been shown to be increased in T2DM patients.[67-69] Interestingly, in spite of its revealing name, the role of IDE in insulin metabolism is not well understood,[70] but implicated in the metabolism of both insulin and Aβ.[70] Additional investigations are warranted to understand the specific role of Cav-1, IR and IDE in Alzheimer's disease pathophysiology or pathogenesis.

We observed severe deficiency in insulin uptake in the absence of Cav-1 expression in brain ECs, as previously observed in cultured lung microvascular ECs.[18] Examination of insulin uptake by ECs using electron microscopy revealed that gold-labelled insulin is taken up by endocytic vesicles that resemble caveolae, whereas insulin uptake was not observed in *Cav-1*$^{-/-}$ mouse brain ECs. Also, formation, swelling and release of caveolae is stimulated by Tyr14 phosphorylation by Src kinase,[71] which is activated downstream of insulin binding to the IR.[18] Thus, activation of insulin signalling can induce caveolae-mediated uptake and transport of receptor-bound insulin as well as fluid-phase cargo molecules. Unlabelled insulin (10×) would not block purely fluid-phase FITC-insulin uptake, nor would pretreatment with unlabelled insulin occlude or occupy receptor sites. A limitation of our study is that FITC-insulin at a concentration lower than 50 nM was undetectable by confocal microscope (Supplementary Fig. 5). This is a challenge given that a detectable concentration is several folds higher than the physiological one, which may result in its binding to IGF-1R, albeit with 100-fold lower affinity compared to its

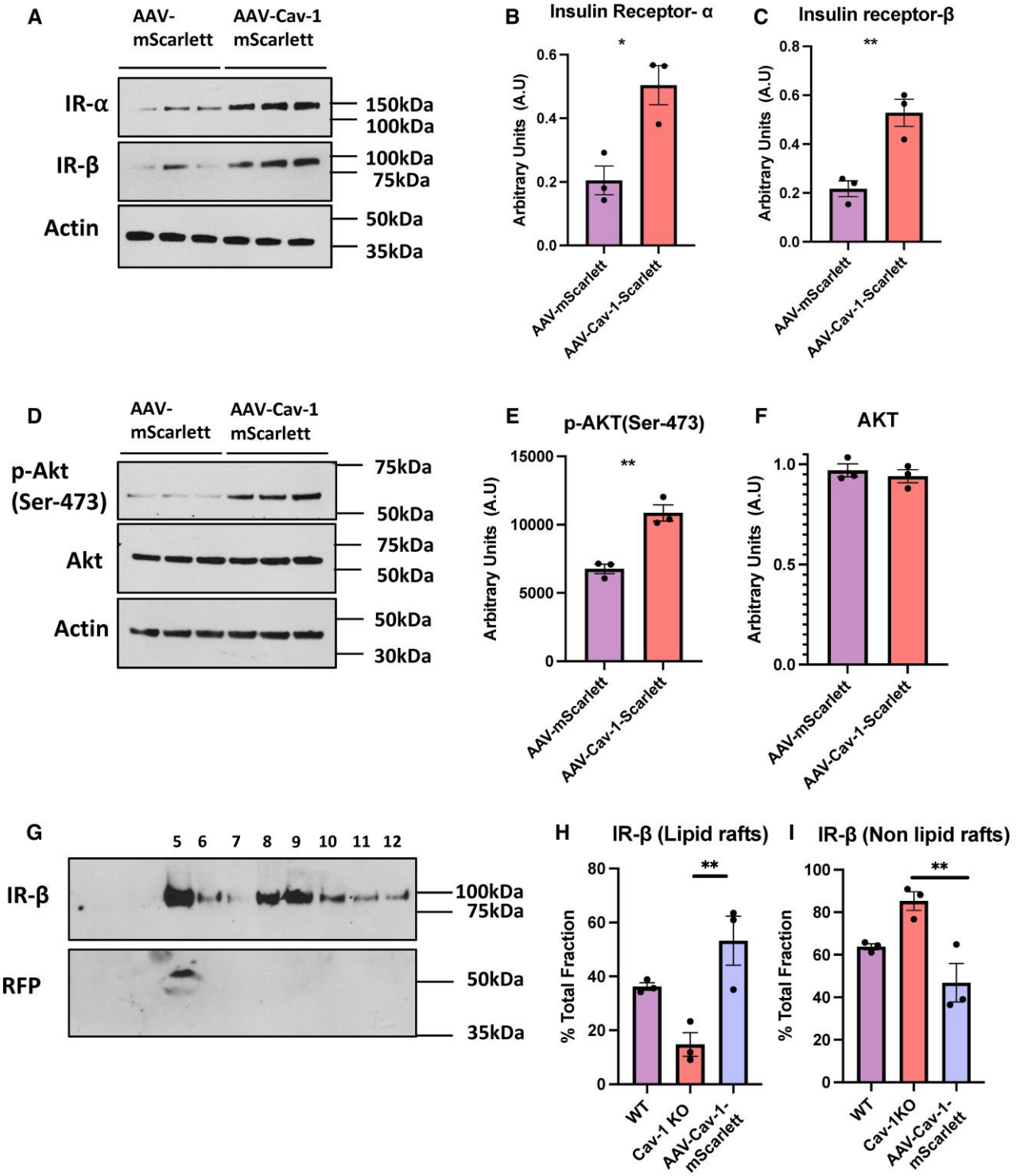

Figure 6 Restoration of Cav-1 expression rescues IR expression and signalling in *Cav-1*$^{-/-}$ ECs. (**A**) Western blot analysis of IR-α and IR-β expression in *Cav-1*$^{-/-}$ bECs infected with AAV-mScarlett or AAV-Cav-1-mScarlett viral vectors. (**B** and **C**) Quantitative analysis of IR-α and IR-β in AAV-mScarlett and AAV-Cav-1-mScarlett infected *Cav-1*$^{-/-}$ bECs. (**D**) Western blot analysis of p-AKT and AKT in *Cav-1*$^{-/-}$ bECs infected with AAV-mScarlett or AAV-Cav-1-mScarlett expression virus followed by insulin stimulation. (**E** and **F**) Quantitative analysis of p-Akt (S473) and AKT following insulin stimulation in Cav-1 knock-out bECs expressing m-Scarlett or Cav-1-mScarlett viral vectors. (**G**) Membrane localization of IR-β and actin in m-Scarlett Cav-1 expressing Cav-1 knock-out bECs ($n = 3$, unpaired *t*-test, $^{*}P < 0.05$, $^{**}P < 0.01$). (**H** and **I**) Quantitative analysis of protein levels of IR-β in different membrane lipid raft fractions isolated from WT, *Cav-1*$^{-/-}$ and Cav-1-mScarlett expressing *Cav-1*$^{-/-}$ bECs ($n = 3$, one-way ANOVA with multiple comparison).

affinity to IR.[72,73] Hence the uptake visualized in the bECs can be driven by high-affinity binding IRs and low-affinity binding IGF-1Rs. Further validation is required in order to discriminate between these scenarios.

Caveolae in brain microvasculature are heterogenous,[74] with brain arteriolar ECs exhibiting abundant caveolae critical for the regulation of neurovascular coupling.[75] On the other hand, although observed by electron microscopy (Supplementary Fig. 8),

their number is limited in brain capillaries due in part to the expression of mfsd2a.[74,76] As there exist no specific markers to separate brain capillary ECs from the artery or venous endothelial cells, additional techniques are required to determine whether insulin uptake is caveolae-mediated throughout the cerebral microvasculature. However, lack of insulin uptake in the absence of Cav-1 observed here affirms its importance in insulin uptake by bECs in general.

The role of Cav-1 in maintenance of membrane protein expression and function, specifically of membrane receptors within lipid rafts, has been described in many cell types including adipocytes[13,37] and ECs.[19] Cav-1 within lipid rafts acts as a scaffold and regulates over 200 signalling pathways.[77] Nevertheless, many important questions remain. Here we showed that Cav-1 specifically interacts with IR-β in ECs and is critical for its stabilization in lipid rafts. Importantly, the lack of Cav-1 shifted the localization of IR-β to the non-lipid raft fraction. We further showed that pathological alterations in insulin signalling are alleviated by restoring Cav-1 expression in *Cav-1*$^{-/-}$ bECs by viral vector transduction.

In conclusion, our study shows that diabetic mice exhibit impaired insulin signalling in brain microvessels and provides evidence that the depletion of Cav-1 in ECs underlies these impairments. This may imply that alterations in Cav-1 regulated insulin trafficking and signalling in the brain can accelerate Alzheimer's pathogenesis. Cav-1 reconstitution strategies may prevent the development of Alzheimer's disease–like neuropathology in patients with type 2 diabetes mellitus.

Acknowledgements

The authors would like to thank laboratory members of the Minshall laboratory for providing critical advice and troubleshooting, specifically, Dr Suellen D.S. Oliveira and Maricela Castellon for providing genotyping protocols for EC-*Cav-1*$^{-/-}$ mice and Dr Zhenlong Chen and Dr Joshua H. Jones for providing advice for FITC- and gold-labelled insulin uptake experiments. The Lazaraov laboratory would like to thank Dr Berislav Zlokovic and his research team for their help with microvessel preparation. We would also like to thank Dr Dan Predescu at Rush University for providing reagents and laboratory space to prepare insulin-labelled gold particles. The authors would like to thank Thu Nguyen for assistance with preparing the manuscript. Some images were prepared using BioRender.com.

Funding

This work is supported by The National Institutes of Health NIA AG060238, AG033570, AG062251, AG076940 (O.L.), HL142636 (R.D.M.), NS114413 and the Together Strong NPC Foundation (S.M.C.), pilot funding from the UIC Center for Clinical and Translational Science (U54 TR002003) and American Heart Association predoctoral fellowship AHA 21PRE836269 (A.S.).

Competing interests

The authors report no competing interests.

Supplementary material

Supplementary material is available at *Brain* online.

References

1. Hameed I, Masoodi SR, Mir SA, Nabi M, Ghazanfar K, Ganai BA. Type 2 diabetes mellitus: From a metabolic disorder to an inflammatory condition. *World J Diabetes*. 2015;6:598.
2. Li X, Song D, Leng SX. Link between type 2 diabetes and Alzheimer's disease: From epidemiology to mechanism and treatment. *Clin Interv Aging*. 2015;10:549-560.
3. De Strooper B, Karran E. The cellular phase of Alzheimer's disease. *Cell*. 2016;164:603-615.
4. Konishi M, Sakaguchi M, Lockhart SM, *et al*. Endothelial insulin receptors differentially control insulin signaling kinetics in peripheral tissues and brain of mice. *Proc Natl Acad Sci*. 2017;114:E8478-E8487.
5. Rhea EM, Banks WA. Role of the blood–brain barrier in central nervous system insulin resistance. *Front Neurosci*. 2019;13:521.
6. Arnold SE, Arvanitakis Z, Macauley-Rambach SL, *et al*. Brain insulin resistance in type 2 diabetes and Alzheimer disease: Concepts and conundrums. *Nat Rev Neurol*. 2018;14:168-181.
7. Denver P, McClean PL. Distinguishing normal brain aging from the development of Alzheimer's disease: Inflammation, insulin signaling and cognition. *Neural Regen Res*. 2018;13:1719-1730.
8. Frölich L, Blum-Degen D, Bernstein HG, *et al*. Brain insulin and insulin receptors in aging and sporadic Alzheimer's disease. *J Neural Transm*. 1998;105:423-438.
9. Ratzmann KP, Hampel R. Glucose and insulin concentration patterns in cerebrospinal fluid following intravenous glucose injection in humans. *Endokrinologie*. 1980;76:185-188.
10. Bell RD, Winkler EA, Singh I, *et al*. Apolipoprotein e controls cerebrovascular integrity via cyclophilin A. *Nature*. 2012;485:512-516.
11. Ernst A, Sharma AN, Elased KM, Guest PC, Rahmoune H, Bahn S. Diabetic *db/db* mice exhibit central nervous system and peripheral molecular alterations as seen in neurological disorders. *Transl Psychiatry*. 2013;3:e263.
12. Niedowicz DM, Reeves VL, Platt TL, *et al*. Obesity and diabetes cause cognitive dysfunction in the absence of accelerated β-amyloid deposition in a novel murine model of mixed or vascular dementia. *Acta Neuropathol Commun*. 2014;2:64.
13. Bonds JA, Shetti A, Bheri A, *et al*. Depletion of caveolin-1 in type 2 diabetes model induces Alzheimer's disease pathology precursors. *J Neurosci*. 2019;39:8576-8583.
14. Cooper-Knock J, Zhang S, Kenna KP, *et al*. Rare variant burden analysis within enhancers identifies *CAV1* as an ALS risk gene. *Cell Rep*. 2020;33:108456.
15. Haddad D, Al Madhoun A, Nizam R, Al-Mulla F. Role of caveolin-1 in diabetes and its complications. *Oxid Med Cell Longev*. 2020;2020:9761539.
16. Cohen AW, Razani B, Wang XB, *et al*. Caveolin-1-deficient mice show insulin resistance and defective insulin receptor protein expression in adipose tissue. *Am J Physiol Cell Physiol*. 2003;285:222-235.
17. Fagerholm S, Örtegren U, Karlsson M, Ruishalme I, Strålfors P. Rapid insulin-dependent endocytosis of the insulin receptor by caveolae in primary adipocytes. *PLoS One*. 2009;4:e5985.
18. Chen Z, Oliveira SDS, Zimnicka AM, *et al*. Reciprocal regulation of eNOS and caveolin-1 functions in endothelial cells. *Mol Biol Cell*. 2018;29:1190-1202.
19. Oliveira SDS, Chen J, Castellon M, *et al*. Injury-induced shedding of extracellular vesicles depletes endothelial cells of cav-1 (caveolin-1) and enables TGF-β (transforming growth factor-β)–dependent pulmonary arterial hypertension. *Arterioscler Thromb Vasc Biol*. 2019;39:1191-1202.
20. Zhao Z, Sagare AP, Ma Q, *et al*. Central role for PICALM in amyloid-β blood–brain barrier transcytosis and clearance. *Nat Neurosci*. 2015;18:978-987.

21. Welser-Alves JV, Boroujerdi A, Milner R. Isolation and culture of primary mouse brain endothelial cells. *Methods Mol Biol*. 2014; 1135:345-356.
22. Marottoli FM, Trevino TN, Geng X, *et al*. Autocrine effects of brain endothelial cell-produced human apolipoprotein E on metabolism and inflammation *in vitro*. *Front Cell Dev Biol*. 2021;9:1431.
23. Wang H, Wang AX, Barrett EJ. Caveolin-1 is required for vascular endothelial insulin uptake. *Am J Physiol Metab*. 2011;300: E134-E144.
24. Predescu D, Qin S, Patel M, Bardita C, Bhalli R, Predescu S. Epsin15 homology domains: Role in the pathogenesis of pulmonary arterial hypertension. *Front Physiol*. 2018;9:1393.
25. Predescu D, Predescu S, Mcquistan T, Palade GE. Transcytosis of α1-acidic glycoprotein in the continuous microvascular endothelium. *Proc Natl Acad Sci U S A*. 1998;95:6175-6180.
26. Quagliarello VJ, Ma A, Stukenbrok H, Palade GE. Ultrastructural localization of albumin transport across the cerebral microvasculature during experimental meningitis in the rat. *J Exp Med*. 1991;174:657-672.
27. Head BP, Patel HH, Roth DM, *et al*. Microtubules and actin microfilaments regulate lipid raft/caveolae localization of adenylyl cyclase signaling components. *J Biol Chem*. 2006;281:26391-26399.
28. Sverdlov M, Shinin V, Place AT, Castellon M, Minshall RD. Filamin A regulates caveolae internalization and trafficking in endothelial cells. *Mol Biol Cell*. 2009;20:4531-4540.
29. Körbelin J, Dogbevia G, Michelfelder S, *et al*. A brain microvasculature endothelial cell-specific viral vector with the potential to treat neurovascular and neurological diseases. *EMBO Mol Med*. 2016;8:609.
30. Maria Nikolakopoulou A, Wang Y, Ma Q, *et al*. Endothelial LRP1 protects against neurodegeneration by blocking cyclophilin A. *J Exp Med*. 2021;218:e20202207.
31. Zeng G, Nystrom FH, Ravichandran LV, *et al*. Roles for insulin receptor, PI3-kinase, and Akt in insulin-signaling pathways related to production of nitric oxide in human vascular endothelial cells. *Circulation*. 2000;101:1539-1545.
32. Zimnicka AM, Husain YS, Shajahan AN, *et al*. Src-dependent phosphorylation of caveolin-1 Tyr-14 promotes swelling and release of caveolae. *Mol Biol Cell*. 2016;27:2090-2106.
33. Werner N, Wassmann S, Ahlers P, Kosiol S, Nickenig G. Circulating CD31+/annexin V+ apoptotic microparticles correlate with coronary endothelial function in patients with coronary artery disease. *Arterioscler Thromb Vasc Biol*. 2006;26:112-116.
34. Sayas CL, Avila J, Wandosell F. Glycogen synthase kinase-3 is activated in neuronal cells by Gα12 and Gα13 by rho-independent and rho-dependent mechanisms. *J Neurosci*. 2002;22:6863.
35. Endo H, Nito C, Kamada H, Yu F, Chan PH. Akt/GSK3 survival signaling is involved in acute brain injury after subarachnoid hemorrhage in rats. *Stroke* 2006;37:2140-2146.
36. Wang H, Wang AX, Liu Z, Barrett EJ. Insulin signaling stimulates insulin transport by bovine aortic endothelial cells. *Diabetes*. 2008;57:540-547.
37. Allen JA, Yu JZ, Dave RH, Bhatnagar A, Roth BL, Rasenick MM. Caveolin-1 and lipid microdomains regulate Gs trafficking and attenuate Gs/adenylyl cyclase signaling. *Mol Pharmacol*. 2009; 76:1082-1093.
38. Czech MP. The nature and regulation of the insulin receptor: Structure and function. *Annu Rev Physiol*. 1985;47:357-381.
39. Morcavallo A, Stefanello M, Iozzo R V, Belfiore A, Morrione A. Ligand-mediated endocytosis and trafficking of the insulin-like growth factor receptor I and insulin receptor modulate receptor function. *Front Endocrinol (Lausanne)*. 2014;5:220.
40. Xiao G, Gan LS. Receptor-mediated endocytosis and brain delivery of therapeutic biologics. *Int J Cell Biol*. 2013;2013:703545.
41. Paccaud JP, Siddle K, Carpentier JL. Internalization of the human insulin receptor. The insulin-independent pathway. *J Biol Chem*. 1992;267:13101-13106.
42. McClain DA, Olefsky JM. Evidence for two independent pathways of insulin-receptor internalization in hepatocytes and hepatoma cells. *Diabetes*. 1988;37:806-815.
43. Fan JY, Carpentier JL, Gorden P, *et al*. Receptor-mediated endocytosis of insulin: Role of microvilli, coated pits, and coated vesicles. *Proc Natl Acad Sci U S A*. 1982;79:7788-7791.
44. Gustavsson J, Parpal S, Karlsson M, *et al*. Localization of the insulin receptor in caveolae of adipocyte plasma membrane. *FASEB J*. 1999;13:1961-1971.
45. Wang X, Yu S, Gao S-J, Hu J-P, Wang Y, Liu H-X. Insulin inhibits aβ production through modulation of APP processing in a cellular model of Alzheimer's disease. *Neuroendocrinol Lett*. 2014;35:224-229.
46. Wang X, Zheng W, Xie JW, *et al*. Insulin deficiency exacerbates cerebral amyloidosis and behavioral deficits in an Alzheimer transgenic mouse model. *Mol Neurodegener*. 2010;5:1-13.
47. Cai W, Zhang X, Batista TM, *et al*. Peripheral insulin regulates a broad network of gene expression in hypothalamus, hippocampus, and nucleus accumbens. *Diabetes*. 2021;70:1857-1873.
48. Soto M, Cai W, Konishi M, Kahn CR. Insulin signaling in the hippocampus and amygdala regulates metabolism and neurobehavior. *Proc Natl Acad Sci U S A*. 2019;116:6379-6384.
49. Chow HM, Shi M, Cheng A, *et al*. Age-related hyperinsulinemia leads to insulin resistance in neurons and cell-cycle-induced senescence. *Nat Neurosci*. 2019;22:1806-1819.
50. Planel E, Tatebayashi Y, Miyasaka T, *et al*. Insulin dysfunction induces *in vivo* tau hyperphosphorylation through distinct mechanisms. *J Neurosci*. 2007;27:13635-13648.
51. King GL, Johnson SM. Receptor-mediated transport of insulin across endothelial cells. *Science*. 1985;227:1583-1586.
52. Bakhshi FR, Mao M, Shajahan AN, *et al*. Nitrosation-dependent caveolin 1 phosphorylation, ubiquitination, and degradation and its association with idiopathic pulmonary arterial hypertension. *Pulm Circ*. 2013;3:816-830.
53. Oliveira SDS, Castellon M, Chen J, *et al*. Inflammation-induced caveolin-1 and BMPRII depletion promotes endothelial dysfunction and TGF-β-driven pulmonary vascular remodeling. *Am J Physiol Lung Cell Mol Physiol*. 2017;312:L760-L771.
54. Lee J, Lee S, Zhang H, Hill MA, Zhang C, Park Y. Interaction of IL-6 and TNF-α contributes to endothelial dysfunction in type 2 diabetic mouse hearts. *PLoS One*. 2017;12:e0187189.
55. Krishnankutty A, Kimura T, Saito T, *et al*. *In vivo* regulation of glycogen synthase kinase 3β activity in neurons and brains. *Sci Rep*. 2017;7:1-15.
56. L'Episcopo F, Drouin-Ouellet J, Tirolo C, *et al*. GSK-3β-induced tau pathology drives hippocampal neuronal cell death in Huntington's disease: Involvement of astrocyte-neuron interactions. *Cell Death Dis*. 2016;7:e2206.
57. Mandyam CD, Schilling JM, Cui W, *et al*. Neuron-targeted caveolin-1 improves molecular signaling, plasticity, and behavior dependent on the hippocampus in adult and aged mice. *Biol Psychiatry*. 2017;81:101-110.
58. Mahmoud AM, Szczurek MR, Blackburn BK, *et al*. Hyperinsulinemia augments endothelin-1 protein expression and impairs vasodilation of human skeletal muscle arterioles. *Physiol Rep*. 2016;4:e12895.
59. Li Y, Zhao Y, Gao C, *et al*. Caveolin-1 derived from brain microvascular endothelial cells inhibits neuronal differentiation of neural stem/progenitor cells *in vivo* and *in vitro*. *Neuroscience*. 2020;448:172-190.
60. Park K, Mima A, Li Q, *et al*. Insulin decreases atherosclerosis by inducing endothelin receptor B expression. *JCI Insight*. 2016;1: 86574.

61. Walker AMN, Warmke N, Mercer B, *et al*. Endothelial insulin receptors promote VEGF-A signaling via ERK1/2 and sprouting angiogenesis. *Endocrinology*. 2021;162:1-15.
62. Maeno Y, Li Q, Park K, *et al*. Inhibition of insulin signaling in endothelial cells by protein kinase C-induced phosphorylation of p85 subunit of phosphatidylinositol 3-kinase (PI3K). *J Biol Chem*. 2012;287:4518-4530.
63. He Z, Opland DM, Way KJ, *et al*. Regulation of vascular endothelial growth factor expression and vascularization in the myocardium by insulin receptor and PI3K/Akt pathways in insulin resistance and ischemia. *Arterioscler Thromb Vasc Biol*. 2006;26:787-793.
64. Kuboki K, Jiang ZY, Takahara N, *et al*. Regulation of endothelial constitutive nitric oxide synthase gene expression in endothelial cells and *in vivo*—A specific vascular action of insulin. *Circulation*. 2000;101:676-681.
65. Zhao Q, Niu Y, Matsumoto K, *et al*. Chotosan ameliorates cognitive and emotional deficits in an animal model of type 2 diabetes: Possible involvement of cholinergic and VEGF/PDGF mechanisms in the brain. *BMC Complement Altern Med*. 2012;12:188.
66. Li Q, Atochin D, Kashiwagi S, *et al*. Deficient eNOS phosphorylation is a mechanism for diabetic vascular dysfunction contributing to increased stroke size. *Stroke*. 2013;44:3183-3188.
67. Kullenberg H, Rossen J, Johansson UB, *et al*. Increased levels of insulin-degrading enzyme in patients with type 2 diabetes mellitus. *Endocrine*. 2022;77:561-565.
68. Šerý O, Zeman T, Hálová A, *et al*. Polymorphism Rs2421943 of the insulin-degrading enzyme gene and the risk of late-onset Alzheimer's disease. *Curr Alzheimer Res*. 2022;19:236-245.
69. Zhang H, Liu D, Huang H, Zhao Y, Zhou H. Characteristics of insulin-degrading enzyme in Alzheimer's disease: A meta-analysis. *Curr Alzheimer Res*. 2018;15:610-617.
70. Leissring MA. Insulin-degrading enzyme: Paradoxes and possibilities. *Cells*. 2021;10:2445.
71. Wang H, Wang AX, Aylor K, Barrett EJ. Caveolin-1 phosphorylation regulates vascular endothelial insulin uptake and is impaired by insulin resistance in rats. *Diabetologia*. 2015;58:1344-1353.
72. De Meyts P, Christoffersen CT, Ursø B, *et al*. Role of the time factor in signaling specificity: Application to mitogenic and metabolic signaling by the insulin and insulin-like growth factor-I receptor tyrosine kinases. *Metab Clin Exp*. 1995;44:2-11.
73. Kjeldsen T, Andersen AS, Wiberg FC, *et al*. The ligand specificities of the insulin receptor and the insulin-like growth factor I receptor reside in different regions of a common binding site. *Proc Natl Acad Sci U S A*. 1991;88:4404-4408.
74. Bonney SK, Coelho-Santos V, Huang S-F, *et al*. Public volume electron microscopy data: An essential resource to study the brain microvasculature. *bioRxiv*. 2022:2022.02.20.481154. doi:10.1101/2022.02.20.481154
75. Chow BW, Nuñez V, Kaplan L, *et al*. Caveolae in CNS arterioles mediate neurovascular coupling. *Nature*. 2020;579:106-110.
76. Andreone BJ, Chow BW, Tata A, *et al*. Blood–brain barrier permeability is regulated by lipid transport-dependent suppression of caveolae-mediated transcytosis. *Neuron*. 2017;94:581-594.e5.
77. Okamoto T, Schlegel A, Scherer PE, Lisanti MP. Caveolins, a family of scaffolding proteins for organizing "preassembled signaling complexes" at the plasma membrane. *J Biol Chem*. 1998;273:5419-5422.